Journal of Power Sources 196 (2011) 2519–2529

Contents lists available at ScienceDirect

Journal of Power Sources

journal homepage: www.elsevier.com/locate/jpowsour

Single-site and nanosized Fe–Co electrocatalysts for oxygen reduction: Synthesis, characterization and catalytic performance

Valentina Bambagioni[a], Claudio Bianchini[a,*], Jonathan Filippi[a], Alessandro Lavacchi[a], Werner Oberhauser[a], Andrea Marchionni[a], Simonetta Moneti[a], Francesco Vizza[a,*], Rinaldo Psaro[b], Vladimiro Dal Santo[b], Alessandro Gallo[c], Sandro Recchia[d], Laura Sordelli[b]

[a] Istituto di Chimica dei Composti Organometallici (ICCOM-CNR), via Madonna del Piano 10, 50019 Sesto Fiorentino, Florence, Italy
[b] Istituto di Scienze e Tecnologie Molecolari (ISTM-CNR), via C. Golgi 19, 20133 Milano, Italy
[c] Istituto di Scienze e Tecnologie Molecolari (ISTM-CNR), via G. Fantoli 16/15, 20138 Milano, Italy
[d] Dipartimento di Scienze Chimiche, Università degli Studi dell'Insubria, Via Valleggio 11, 22100 Como, Italy

ARTICLE INFO

Article history:
Received 15 July 2010
Received in revised form 20 October 2010
Accepted 7 November 2010
Available online 12 November 2010

Keywords:
Iron
Cobalt
Phthalocyanine
Electrocatalysts
Oxygen reduction
Fuel cells

ABSTRACT

The impregnation of Ketjen Black (C) with iron and cobalt phthalocyanines (*MPc*) taken one by one or as a 1:1 stoichiometric mixture, followed by heat treatment at 600 °C under inert atmosphere, gave materials containing arrays of single metal ions coordinated by four nitrogen atoms (M-N_4 units). Increasing the pyrolysis temperature to 800° resulted in the formation of carbon-supported, nanosized metal particles. A key role of the carbon support in determining the material structure at either temperature investigated was demonstrated by TPD, EXAFS, XANES and XRPD studies. These also showed that a Fe–Co alloy is obtained at 800 °C when the impregnation of Ketjen Black involves a mixture of *FePc* and *CoPc*. Electrodes coated with the different Fe, Co and Fe–Co materials, containing ca. 3 wt% metal loadings, were scrutinized for the oxygen reduction reaction (ORR) in alkaline media by linear sweep voltammetry. For comparative purposes, two Pt electrocatalysts containing 3 and 20 wt% metal were investigated. The electrochemical activity of all materials was analyzed by Tafel and Koutecky–Levich plots as well as chronopotentiometry. The Fe-containing electrocatalysts have been found to be highly active for the ORR in alkaline media with convective limiting currents as high as 600 A g Fe^{-1} at room temperature and onset potentials as high as 1.02 V vs. RHE. It has been found that (i) the ORR mass activity of the *Pc*-derived electrocatalysts is superior to that of the Pt catalysts investigated; (ii) the activity of *FePc* and *FePc–CoPc/C*, heat treated at either 600 or 800 °C, is superior to that of the corresponding Co materials; (iii) the electrocatalysts obtained at 600 °C are fairly more active than those obtained at 800 °C.

1. Introduction

Since the pioneer work by Jasinski in 1964 [1], cobalt and iron complexes with phthalocyanines (*Pc*) or similar *N*-macrocycles, supported on carbon blacks, have been largely used as electrocatalysts for the oxygen reduction reaction (ORR), either in the molecular form [2–12] or after thermal treatment under inert atmosphere [13–21]. Within the latter context, the pyrolysis temperature has been found to be a crucial parameter to determine the structure of metallophthalocyanine-derived electrocatalysts and, consequently, their electrochemical performance. It is now apparent that pyrolysis temperatures around 600 °C lead to the prevalent formation of M-N_4 units with the metals predominantly in the +2 oxidation state, while metal particles are obtained at higher temperatures, around 800 °C [13–21]. Either morphology is active for the ORR in both alkaline and acidic media, yet the electrocatalysts are more stable in the former environment [16,22,23]. As a matter of fact, *MPc*-derived electrocatalysts are overwhelming any other material, including Pt, for alkaline direct alcohol fuel cells (DAFCs), in terms of both cost and performance [23].

In this paper, we describe the synthesis and characterization of a family of electrocatalysts based on iron phthalocyanine (*FePc*), cobalt phthalocyanine (*CoPc*) and mixtures thereof. To the best of our knowledge, electrocatalysts obtained by mixing *FePc* and *CoPc* have not been reported so far. Likewise, the conductive carbon used in this work, Ketjen Black, has been scarcely investigated as support for *MPc*-based electrocatalysts [12].

A multiform study, encompassing Temperature-Programmed Decomposition (TPD), Extended X-ray Absorption Fine Structure Spectroscopy (EXAFS), Near Edge X-ray Absorption Spectroscopy (XANES), X-ray Powder Diffraction (XRPD) and various analytical

* Corresponding author. Tel.: +39 0555225280; fax: +39 0555225203.
E-mail addresses: claudio.bianchini@iccom.cnr.it (C. Bianchini), francesco.vizza@iccom.cnr.it (F. Vizza).

0378-7753/$ – see front matter © 2010 Elsevier B.V. All rights reserved.
doi:10.1016/j.jpowsour.2010.11.030

techniques, has provided us with a reliable picture of their structure as well as the mechanism leading to the formation of the electroactive phases. The electrochemical activity of all catalysts towards the ORR in alkaline media has been investigated and compared to that of proprietary or commercial Pt catalysts.

2. Experimental

2.1. Materials and general instrumentation

All manipulations, except as stated otherwise, were routinely performed under a nitrogen atmosphere using standard airless technique. Ketjen Black (EC-600JD) was purchased from Akzo Nobel. *Pt/Vulcan* (Pt 20 wt%) was purchased from E-TEK. All the solutions were freshly prepared with doubly distilled-deionized water. The sonication process was made with a Bandelin Sonopuls probe instrument.

Prior to deposition of Fe and/or Co phthalocyanines, the carbon support (5 g) was treated with 400 mL of a 1:1 (v:v) mixture of 98% H_2SO_4 and 70% HNO_3 for 24 h at room temperature, followed by washing with deionized water and dried over night at 60 °C under reduced pressure. All metal salts and reagents were purchased from Aldrich and used as received. SiO_2 (mesoporous, amorphous support, SSA = 330 $m^2\,g^{-1}$) was purchased from Grace. The quartz power (fine granular, washed and calcined GR for analysis) was purchased from Merck. Iron(II) and cobalt(II) phthalocyanines were purchased from Aldrich and used as received.

Temperature Programmed Decomposition (TPD) experiments were carried out under a helium flow (5.0 purity, further purified by a Supelco gas purifier) at 10 mL min^{-1} and a heating rate of 5 °C min^{-1}. The gaseous products were analyzed by an on-line QMS (MASSTORR FX, 0–100 amu) connected downstream; the solid products condensed on the reactor cold walls were further analyzed by GC–MS (HP 5890 series II GC – HP 5971 series mass selective detector) and by CHN analysis (Perkin Elmer 2400).

The metal contents were determined by ion chromatography. Each sample (50 mg) was treated in a microwave heated digestion bomb in sealed PTFE vessels with concentrated HNO_3 (2.0 mL) and 98% H_2SO_4 (2 mL). The heating program comprised some preheating steps and a final 10 min digestion step at 220 °C. After the carbon residue was filtered off, the solutions were analyzed using an ion-chromatographic apparatus (Metrohm, 761 model) equipped with a post-column derivatization system and UV detector.

EXAFS measurements have been carried out at the XAFS beamline at the Elettra synchrotron facility in Basovizza (Trieste) by means of a double-crystal Si(1 1 1) monochromator. All samples, pure mono and bi-metallic complexes, systems after carbon impregnation and after pyrolysis, have been measured in transmission mode at RT at both metal edges. Iron and Cobalt foil and Fe(II) and Co(II) acetates have been used as reference materials for the experimental phase and amplitude function extraction. Spectra, recorded over samples loaded into sample-holders in a dry-box under N_2 atmosphere at the end of each treatment, have been acquired at room temperature and at least three scans per spectrum have been averaged in order to improve the signal-to-noise ratio and to evaluate the error bars. Data analysis has been performed with the FEFF8 software package. The experimental $\chi(k)$ functions have been extracted from the absorption spectra through a standard procedure of subtraction of the pre-edge and fit evaluated monoatomic background, and normalization to the edge jump with the Langeler method. The so obtained signals, multiplied by a proper function (Kaiser window $\tau = 3$), have been Fourier transformed over the k 2.5–15 $Å^{-1}$. The FFT convolution peaks, representing the radial distribution of the scattering atoms around the absorbing element, have been back filtered and fitted k1-space by the non-linear, least-squares, multiple scattering IFEFF application.

X-ray Powder Diffraction spectra were acquired at room temperature with a PANalytical X'PERT PRO diffractometer, employing $Cu_{K\alpha}$ radiation (λ = 1.54187 Å) and a parabolic MPD-mirror. The spectra were acquired in the 2Θ range from 5.0 to 120.0°, using a continuous scan mode with an acquisition step size of 0.0263° and a counting time of 49.5 s. The "in situ" thermo-diffraction study was carried with an Anton Paar (HTK 1200) high temperature reaction chamber applying nitrogen and argon as inert gases an applying a heating rate of 15 °C min^{-1}.

2.2. Electrochemical measurements

In the linear sweep voltammetry was used a Pyrex™ (Princeton Applied Research) glass cell filled with a 0.1 M KOH solution into which O_2 was bubbled (30 mL min^{-1}) for 30 min prior to each experiment. The reference electrode was a commercial $Ag/AgCl/KCl_{sat}$ (Princeton Applied Research) with a potential of +197 mV respect to the NHE. The counter electrode was a platinum gauze enclosed in a glass tube with porous bottom. All electrochemical studies were carried out using a Parstat 2277 potentiostat–galvanostat (Princeton Applied Research) equipped with Model 616 Rotating Disk Electrode (PAR/Ametek).

2.2.1. Ink preparation

A portion (48 mg) of each electrocatalyst was placed in a high density polyethylene vessel together with 2.2 g of anhydrous THF and 0.19 g of a Tokuyama™ OH-type anion exchange resin in alcohol solution. The resulting suspension was sonicated for 1 h with a FALC sonic bath and then introduced into a 5 mm (A = 0.1963 cm^2) teflon potted glassy-carbon rotating disk electrode tip (PINE™) by means of a 5 μl micro-pipette. Each suspension was freshly prepared just before carrying out the experiment scheduled. The amount of ink was weighted by means of an analytical balance. Each electrode was dried for 30 min before it was mounted on the rotating disk electrode shaft and then immersed into the O_2 saturated solution. Linear sweep voltammetry experiments were carried out at an electrode rotating speed of 1600 rpm (except for the Levich plot experiments where the speed varied from 400 to 2600 rpm). The potential was swept from +200 mV vs. Ag|AgCl|KClsat (close to the OCV of the electrode in the same conditions) to −400 mV, below the potential at which the convective current limit was reached. A sweeping rate of 5 mV s^{-1} was applied, which is slow enough to ensure a steady state in each point of the curve. Chronopotentiometric experiments were carried out by imposing a constant cathodic current of 2.5 mA cm^{-2} measuring the variation of the potential of the electrode with the time; the solution was saturated by continuous O_2 bubbling.

2.3. Electrocatalysts preparation

2.3.1. Preparation of FePc/C, FePc/C (600) and FePc/C (800)

Ketjen Black (5 g) was added to a suspension of FePc (2.3 g) in THF (200 mL) that had previously stirred for 30 min at room temperature and then sonicated for 30 min. The resulting mixture was stirred at room temperature for 2 h. Afterwards, the solvent was removed under reduced pressure and the solid residue of *FePc/C* was dried under high vacuum (yield 7.1 g). *FePc/C* (7.0 g) was introduced into to a quartz tube and heated at 600 °C (20 °C min^{-1}) or 800 °C (20 °C min^{-1}) under a flow of nitrogen (1 L min^{-1}) for 2 h. After cooling to room temperature under a nitrogen flow, the resulting black material, *FePc/C (600)* (yield 6.5 g) or *FePc/C (800)* (yield 5.9 g) was removed and stored under nitrogen.

2.3.2. Preparation of CoPc/C, CoPc/C (600) and CoPc/C (800)

Ketjen Black (5 g) was added to a suspension of CoPc (2.3 g) in THF (200 mL) that had previously stirred for 30 min at room temperature and then sonicated for 30 min. The resulting mixture was stirred at room temperature for 2 h. Afterwards, the solvent was removed under reduced pressure and the solid residue of *CoPc/C* was dried under high vacuum (yield 7.2 g). *CoPc/C* (7.0 g) was introduced into to a quartz tube and heated at 600 °C (20 °C min^{-1}) or 800 °C (20 °C min^{-1}) under a flow of nitrogen (1 L min^{-1}) for 2 h. After cooling to room temperature under a nitrogen flow, the resulting black material, *CoPc/C (600)* (yield 6.6 g) and *CoPc/C (800)* (yield 6.2 g) was removed and stored under nitrogen.

2.3.3. Preparation of FePc–CoPc/C, FePc–CoPc/C (600) and FePc–CoPc/C (800)

Ketjen Black (5 g) was added to an equimolar mixture of FePc (1.15 g) and *CoPc/C* (1.15 g) in THF (100 mL) that had previously stirred for 30 min at room temperature and further sonicated for 30 min. The solvent was then removed under reduced pressure and the solid residue of *FePc–CoPc/C* was dried under high vacuum. (yield 7.2 g). *FePc–CoPc/C* (7.0 g) was introduced into to a quartz tube and heated at 600 °C (20 °C min^{-1}) or 800 °C (20 °C min^{-1}) under a flow of nitrogen (1 L min^{-1}) for 2 h. After cooling to room temperature under a nitrogen flow, the resulting black material of *FePc–CoPc/C (600)* (yield 6.8 g) or *FePc–CoPc/C (800)* (yield 6.4 g) was removed and stored under nitrogen.

2.3.4. Preparation of FePc/SiO_2, CoPc/SiO_2 and FePc–CoPc/SiO_2

Mesoporous SiO_2 (0.5 g) was added to a THF suspension of FePc (0.265 g) or CoPc (0.256 g) or a mixture FePc (0.141 g) and CoPc (0.110 g) sonicated for 20 min. The resulting slurry was sonicated for 40 min, then the solvent was removed under reduced pressure and the solid residue was dried under high vacuum. Yields *FePc/SiO_2* 0.71 g, *CoPc/SiO_2* 0.72 g and *FePc–CoPc/SiO_2* 0.71 g.

2.3.5. Preparation of FePc/quartz or CoPc/quartz

FePc (0.024 g) or *CoPc* (0.023 g) was added to 0.033 g of quartz powder and the mixture was thoroughly grinded in a mortar.

2.3.6. Preparation of Pt/C

Ketjen Black (3 g) was sonicated for 20 min in a 500 mL three-necked flask containing ethylene glycol (400 mL). A solution of H_2PtCl_6 (0.235 g, 0.453 mmol) in ethylene glycol (50 mL) and water (50 mL) was added dropwise to the resulting suspension with stirring. Successively, a solution of NaOH (5.6 g) in water (40 mL) was introduced into the reactor which was then heated to 140 °C under a nitrogen atmosphere. After 3 h, the reaction mixture was allowed to cool to room temperature and the solid product was filtered off and washed with distilled water to neutral pH. The final product was dried at 50 °C under vacuum to constant weight. Yield 3.2 g ICP-AES (wt%): Pt 3.2.

3. Results and discussion

3.1. Synthesis of precursors and electrocatalysts

Ketjen Black (*C*) was impregnated with *FePc*, *CoPc* or their equimolar mixture by stirring THF suspensions of the latter complexes with the carbon material, followed by separation and drying under reduced pressure. As shown by specific characterization techniques (*vide infra*), an excellent dispersion of the starting metal complexes was obtained, which is most likely due to strong π-graphene and σ-oxygen interactions of the *MPc* moieties with the carbon surface [24–27]. The resulting materials, *FePc/C*, *CoPc/C* and *FePc–CoPc/C* were collected and adequately characterized (*vide infra*). Next, the latter products were pyrolyzed under nitrogen at 600 or 800 °C to give the electrocatalysts *FePc/C(600)*, *CoPc/C(600)*, *FePc–CoPc/C(600)*, *FePc/C(800)*, *CoPc/C(800)* and *FePc–CoPc/C(800)*, respectively.

Table 1
Elemental analysis (C, H, N, Fe or Co) of the material employed or synthesized in this work.

Sample	*T* (°C)	C (wt%)	H (wt%)	N (wt%)	Co (wt%)	Fe (wt%)
KetJen Black	RT	96.60	0.44	0.09		
FePc	RT	64.61	2.77	18.50		
CoPc	RT	66.94	2.82	19.45		
	RT	82.50	1.69	5.08		3.10
FePc/C	600	87.94	0.62	3.47		2.88
	800	91.31	0.40	1.36		3.02
	RT	86.54	1.49	5.96	3.10	
CoPc/C	600	88.09	0.76	5.33	3.10	
	800	87.51	0.93	3.65	3.29	
	RT	84.53	1.58	5.54	1.80	1.40
FePc–CoPc/C	600	88.24	0.88	4.88	1.64	1.06
	800	90.62	0.54	2.48	1.72	1.13

Table 1 reports selected elemental analysis data of both precursors and final electrocatalytic materials. Irrespective of the starting reagent and synthetic procedure, all samples were found to contain an overall metal content of ca. 3 wt%.

For comparing the deposition and thermal decomposition of the phthalocyanines, some model materials with a comparable metal loading were prepared using an inert support material. Stirring acetone suspensions of *FePc*, *CoPc* or their equimolar mixture in the presence of mesoporous silica gave *FePc/SiO_2*, *CoPc/SiO_2* and *FePc–CoPc/SiO_2*, while *FePc/quartz* and *CoPc/quartz* were straightforwardly obtained by grinding appropriate amounts of either *FePc* or *CoPc* with quartz powder.

3.2. Characterization

3.2.1. Temperature-Programmed Decomposition (TPD)

In addition to elemental analysis, all materials were characterized by TPD (Fig. 1) and the decomposition products were identified by various methods. The gaseous products were analyzed by an on-line mass-spectrometer connected downstream, monitoring the following mass channels: $m/z = 2$ (H_2^+); $m/z = 14$ (N^+, CH_2^+); $m/z = 15$ (CH_3^+); $m/z = 27$ (HCN^+); $m/z = 28$ (N_2^+, CO^+, $C_2H_4^+$); $m/z = 43$ (CH_3CO^+); $m/z = 77$ ($C_6H_5^+$). The solid products, condensed on the reactor walls, were identified by GC–MS and CHN analysis.

All the samples supported on Ketjen Black showed the evolution of the impregnation solvent, THF, at ca. 100 °C. At higher temperature, two peaks were observed for the $m/z = 2$ mass channel: one at 570 and 640 °C for *FePc/C* and *CoPc/C*, respectively, the other at 770–780 °C for both metals. Different peak temperatures for Fe and Co were also observed for the $m/z = 27$ mass channel. Indeed, the TPD profile of *FePc/C* showed a peak at 567 °C and a more intense peak at 777 °C, whereas the profile of *CoPc/C* pyrolysis showed only a peak at 805 °C. Notably, no trace of benzene evolution was observed for either metal.

In view of the analysis of the gaseous product evolved in the temperature interval from 570 to 800 °C, one may conclude that Fe and Co drive slightly different decomposition paths. The influence of the metal center in determining the decomposition of the *Pc* framework was definitely confirmed by the analysis of the products desorbed upon TPD and collected on the reactor walls. This study has provided evidence of the importance of the carbon support on the thermal decomposition mechanism. Indeed, the decomposition product of *CoPc/C* was selectively 1,2-benzodinitrile, while the pyrolysis of *FePc/C* gave 1,2-benzodinitrile and phthalimide approximately in a 1:1 ratio (Table 2). As a convincing evidence of

Table 2
Condensed products upon pyrolysis of the Fe and Co phtalocyanines supported on various materials in the temperature range from 600 to 800 °C.[a]

Sample	Phthalocyanine	1,2-Benzodinitrile	Phthalimide
CoPc/C	–	++	–
FePc/C	–	++	++
FePc–CoPc/C	–	++	++
CoPc/quartz	++	–	–
FePc/quartz	++	–	–
CoPc/SiO_2	++	+	+
FePc/SiO_2	++	+	+
FePc–CoPc/SiO_2	++	+	+

[a] –, not detected; +, detected in low amount; ++, detected in high amount.

the importance of the carbon support in driving the pyrolysis path, the TPD of *FePc/quartz* and *CoPc/quartz* gave the intact *Pc* ligand as sublimate product (Table 2). Intact *Pc* was also the largely major product released upon pyrolysis of the silica-supported complexes *FePc/SiO_2*, *CoPc/SiO_2* and *FePc–CoPc/SiO_2* up to 800 °C (Table 2).

On the basis of the TPD profiles and of the decomposition products, one may realize that the temperatures of 570 and 800 °C are representative of two different stages of the decomposition process of *FePc/C* and *CoPc/C*: a partial decomposition of the metal complexes would occur in the temperature interval between the first peak of the $m/z = 2$ mass channel and the second peak in the $m/z = 27$ profile, while a full decomposition of the *Pc* framework, with formation of metal particles (*vide infra*), would occur around 800 °C at which all the evolution peaks are "closed". Consistent with this hypothesis, a much lower nitrogen content was found in the pyrolyzed products at 800 °C (Table 1). It is also worth noticing that the decrease in the nitrogen content was much higher for the Fe-containing materials (Table 1), which is in line with the evolution of both 1,2-benzodinitrile and phthalimide (Table 2).

A GC–MS analysis of the nonvolatile products obtained upon thermal decomposition (300–600 °C) under nitrogen of *FePC* and *CoPc* supported on Vulcan XC-72 has been previously reported [13]. In either case, both phthalimide and 1,2-benzodinitrile were detected. On the other hand, when *CoPc* is not supported on a carbon black, as is the case of a *CoPc* sheet polymer, the pyrolysis gave no phthalimide but only 1,2-benzodinitrile together with other nitrogen products (HCN, $(CN)_2$, C_6H_5CN) [28]. In view of the results reported in Table 1 as well as previous literature evidence, one may therefore conclude that the presence of oxygenated groups on the support surface, as in Ketjen Black or Vulcan-XC72 [24–26] is mandatory to produce phthalimide upon thermal decomposition of iron and cobalt phthalocyanines.

3.2.2. Extended X-ray Absorption Fine Structure Spectroscopy (EXAFS) and Near Edge X-ray Absorption Spectroscopy (XANES)

The materials investigated by EXAFS and XANES are listed in Tables 3 and 4 that also summarize the best fit results at the Fe and Co K-edges, respectively. Comparisons of the XANES spectra and of the Fourier transformed EXAFS spectra at both edges are reported for each sample in Figs. 2–7, respectively. XANES showed unambiguously that, upon deposition over Ketjen Black, the coordination geometry around Fe and Co, originally square-planar, changes to square pyramidal. Indeed, the pre-edge peak at higher energy disappeared in favour of the component on its left for iron, while an intensity decrease was observed for cobalt. This experimental observable may be attributed to a symmetry decrease from D_{4h} to C_{4v}, corresponding to a geometry change from square planar with four nitrogen donor atoms to square pyramidal with four basal nitrogen atoms and one apical donor (Figs. 2A and 3A), most likely an oxygen atom (Tables 3 and 4). In this respect, it is worth recalling that, unlike Fe(II) complexes, both square-planar and square-pyramidal Co(II) complexes with four nitrogen ligands have low-spin configuration [29,30]. In actuality, the fit calculations do not allow one to discriminate unambiguously between N or O as scattering atoms, which means that both "5N" and "4N+1O" structure may be equally possible. On the other hand, the absence of a significant amount of nitrogen atoms on the carbon surface (Table 1), which is, in fact, rich of oxygenated species (–COOH, –OH) upon treatment with H_2SO_4/HNO_3 [24–27], decreases substantially

Table 3
EXAFS best fit results at the Fe K-edge and estimated metal particle average diameter.

Sample	Shell	*N*	*R* (Å)	σ_{DW} (Å)
FePc	Fe–N	4.0	1.93	0.046
	Fe–C	8.0	2.99	0.077
	Fe–N	4.0	3.40	0.089
FePc/C	Fe–N	4.0	1.91	0.068
	Fe–O	1.0	2.08	0.021
	Fe–C	8.0	2.98	0.089
	Fe–N	4.0	3.41	0.070
FePc–CoPc/C	Fe–N	4.0	1.92	0.070
	Fe–O	1.0	2.09	0.029
	Fe–C	8.0	3.03	0.067
	Fe–N	4.0	3.43	0.060
FePc–CoPc/C(600)	Fe–N	4.0	1.92	0.068
	Fe–O	0.9	2.09	0.028
	Fe–C	7.8	3.03	0.057
	Fe–N	3.6	3.44	0.028
FePc–CoPc/C(800)	Fe–N	2.0	1.93	0.035
	Fe–M	3.1	2.49	0.084
	Fe–C	4.0	2.91	0.054
	Fe–N	2.0	3.44	0.072
FePc–CoPc/SiO_2	Fe–N	4.0	1.93	0.046
	Fe–C	8.0	2.99	0.077
	Fe–N	4.0	3.40	0.089
FePc/SiO_2	Fe–N	4.0	1.93	0.046
	Fe–C	8.0	2.99	0.077
	Fe–N	4.0	3.40	0.089

Table 4
EXAFS best fit results at the Co K-edge and estimated metal particle average diameter.

Sample	Shell	*N*	*R* (Å)	σ_{DW} (Å)
CoPc	Co–N	4.0	1.91	0.045
	Co–C	8.0	2.96	0.069
	Co–N	4.0	3.35	0.051
CoPc/C	Co–N	4.0	1.90	0.048
	Co–O	1.0	1.99	0.013
	Co–C	8.0	2.95	0.068
	Co–N	4.0	3.42	0.097
FePc–CoPc/C	Co–N	4.0	1.92	0.040
	Co–O	1.0	2.04	0.022
	Co–C	8.0	2.97	0.075
	Co–N	4.0	3.40	0.096
FePc–CoPc/C(600)	Co–N	4.0	1.92	0.045
	Co–O	1.0	2.02	0.019
	Co–C	8.0	2.99	0.068
	Co–N	4.0	3.41	0.081
FePc–CoPc/C(800)	Co–N	2.5	1.94	0.035
	Co–M	3.3	2.48	0.086
	Co–C	4.8	2.95	0.054
	Co–N	2.6	3.42	0.072
CoPc/SiO_2	Co–N	4.0	1.93	0.046
	Co–C	8.0	2.95	0.062
	Co–N	4.0	3.39	0.098
FePc–CoPc/SiO_2	Co–N	4.0	1.92	0.048
	Co–C	8.0	2.96	0.069
	Co–N	4.0	3.41	0.095

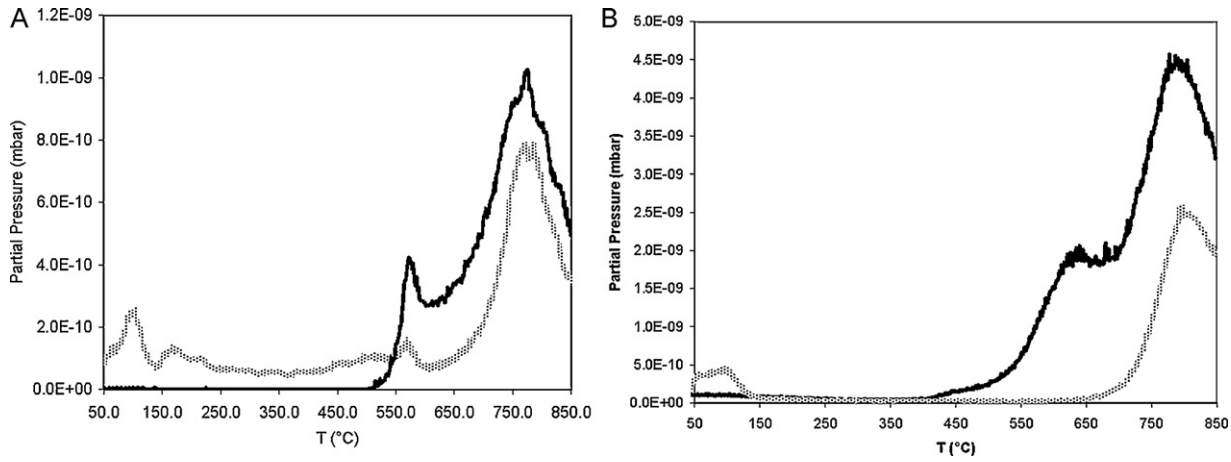

Fig. 1. TPD profiles at the $m/z = 2$ (black line) and $m/z = 27$ (grey line) mass channels of *FePc/C* (a) and *CoPc/C* (b).

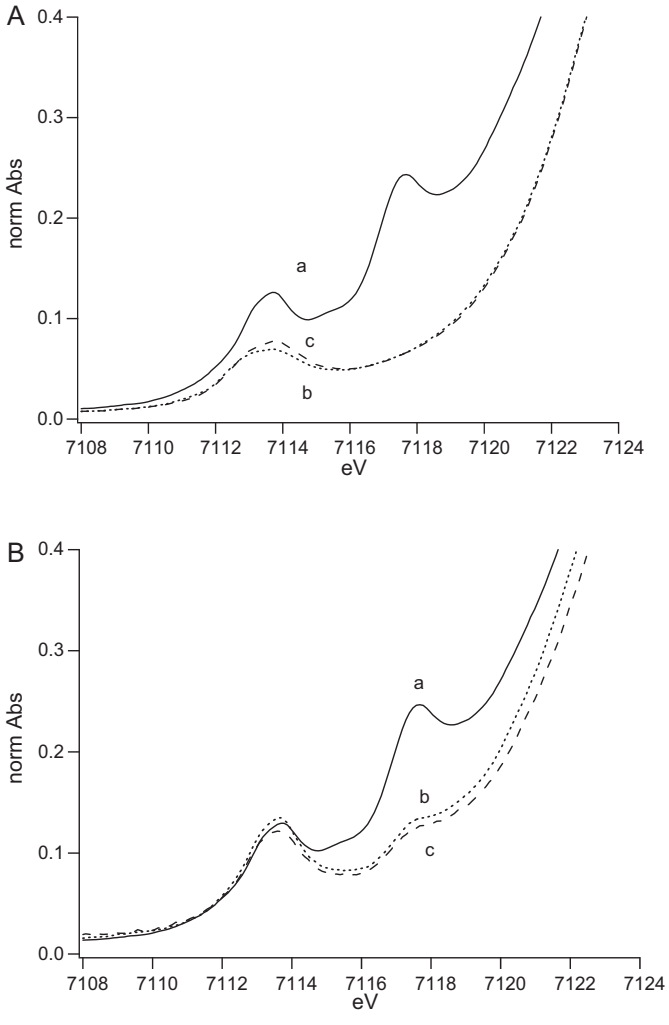

Fig. 2. (A) Fe K-edge normalised XANES spectra of: (a) *FePc* (—), (b) *FePc/C* (...), (c) *FePc–CoPc/C* (- - -). (B) Fe K-edge normalised XANES spectra of: (a) *FePc* (—), (b) *FePc/SiO₂* (...), (c) *FePc–CoPc/SiO₂* (- - -).

the probability that the apical donor atom of the square pyramids may be nitrogen. For this reason, an oxygen atom has been introduced in Tables 3 and 4 as the fifth atom that completes the metal coordination sphere (Scheme 1).

It is noteworthy that the X-ray absorption spectra at both Fe and Co edges of the carbon supported complexes did not change when *FePc* or *CoPc* were deposited independently or simultaneously (Figs. 2A and 3A). A change of the initial D_{4h} symmetry of *FePc* upon impregnation on Vulcan XC-72 has been also observed by Mössbauer and Raman spectroscopies [31].

A perusal of the EXAFS spectra reported in Figs. 4A and 5A confirms that the characteristic shell trend of the starting *Pc* complex is affected by the deposition on Ketjen Black: an increase of the nearest neighbour contribution is much more evident at the Fe edge, together with a distortion of the Fe–C and Fe–N distances in the next nearest shells, as compared to the Co edge. However, the XANES and EXAFS spectra suggest that both the Fe and Co atoms in the starting *Pc* complexes interact with the support surface so as to adopt a square-pyramidal, most likely 4N+1O, structure.

The role played by the carbon support, through its surface groups, in modifying the coordination geometry around the metal center, was unequivocally demonstrated by EXAFS on the analogous *MPc* complexes supported on SiO_2: in this case, in fact, the *Pc* neighbours shell trend in the EXAFS spectra (Figs. 4B and 5B) was totally unaffected by the impregnation over the oxide support.

Upon pyrolysis of *FePc–CoPc/C* at 800 °C under N_2, a drastic structural change was observed: most of the isolated metal ions disappeared, formed in their place were small metal particles (ca. 1–2 nm). This phenomenon is illustrated in Figs. 6B and 7B: both metals were partly reduced in a *bcc* metal phase to give Fe–Co alloy metal particles with an average size of about 8 Å. A fraction of both iron and cobalt were still present as oxygen surrounded atoms,

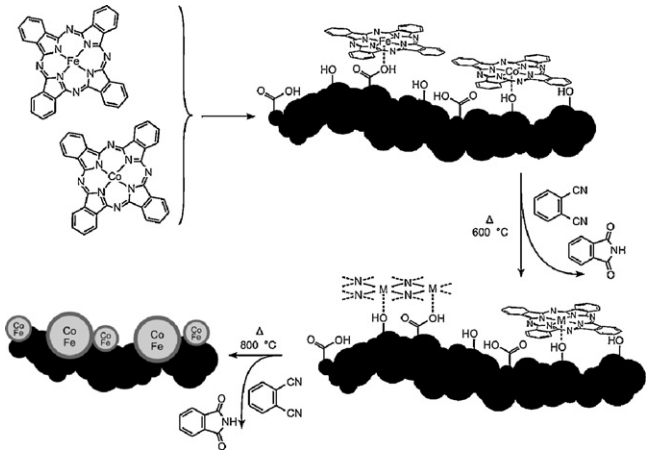

Scheme 1. Proposed mechanism for the pyrolysis of Fe and Co phthalocyanines supported on Ketjen Black.

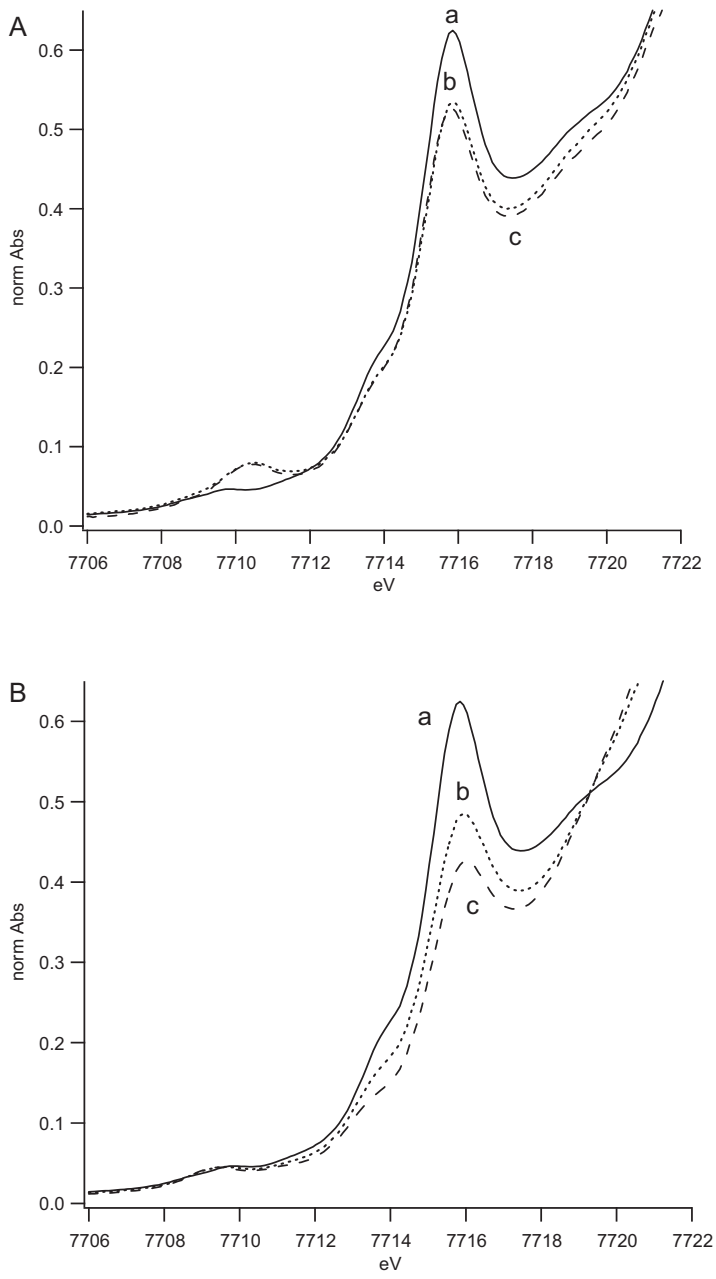

Fig. 3. (A) Co K-edge normalised XANES spectra of: (a) *CoPc* (___), (b) *CoPc/C* (...), (c) *FePc–CoPc/C* (- - -). (B) Co K-edge normalised XANES spectra of: (a) *CoPc* (___), (b) *CoPc/SiO_2* (...), (c) *FePc–CoPc/SiO_2* (- - -).

most probably small oxidic aggregates. The corresponding XANES spectra (Figs. 6A and 7A) showed the presence of both M^{2+} ions and M^0 species. Consistent with both the TPD and XRPD experiments (see below), the pyrolysis of *FePc–CoPc/C* at 600 °C under N_2 led to a minor decomposition of the supported complexes as the first shell contribution (N or O) was still present (Figs. 6B and 7B).

XANES and EXAFS studies at the Co K-edge of pure *CoPc* and *CoPc* supported on Vulcan XC-72, before and after heat treatment, have been previously reported [14]. In line with our results, the Co–N_4 structure was retained up to 700 °C. Above this temperature, only metallic cobalt particle were detected. A similar behavior has been reported for pure *FePc* [15]. Like for the present *FePc/C* material, the fine structures, due to the $1s \rightarrow 4p$ transitions, typical of the Fe–N_4 structure, disappeared above 600 °C and metal oxide began to form.

3.2.3. X-ray Powder Diffraction (XRPD) analysis

The morphology of *FePc/C*, *CoPc/C* and *FePc–CoPc/C* was investigated by XRPD carried out from room temperature to 600 °C. The XRPD-spectra at room temperature showed the typical pattern of the carbon support with two very broad diffraction peaks centered at ca. 25 and 43° [32], which is consistent with the presence of an amorphous phase of the *MPc* species. Traces a and b of Fig. 8 illustrate this behavior for *FePc–CoPc/C*.

XRPD spectra acquired after a temperature-controlled heating of *FePc/C*, *CoPc/C* and *FePc–CoPc/C* to 600 °C in a heating oven under a nitrogen atmosphere showed the absence of any crystalline phase deriving from the decomposition of the supported metal complexes. In Fig. 8, trace c, is shown a representative XRPD pattern after heating *FePc–CoPc/C* to 600 °C. A similar behavior was displayed by the single metal materials *FePc/C* and *Co/Pc*.

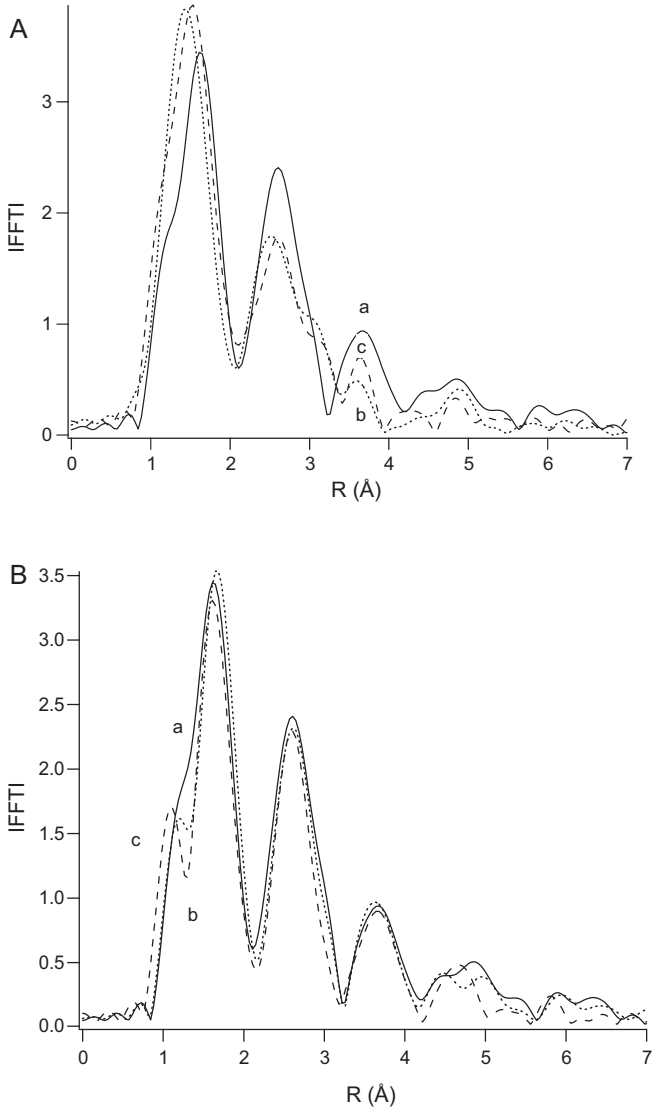

Fig. 4. (A) Fe K-edge Fourier transforms EXAFS spectra (k^3-weighed, not phase corrected) of: (a) *FePc* (___), (b) *FePc/C* (..), (c) *FePc–CoPc/C* (- - -). (B) Fe K-edge Fourier transforms EXAFS spectra (k^3-weighed, not phase corrected) of: (a) *FePc* (___), (b) *FePc/SiO_2* (...), (c) *FePc–CoPc/SiO_2* (- - -).

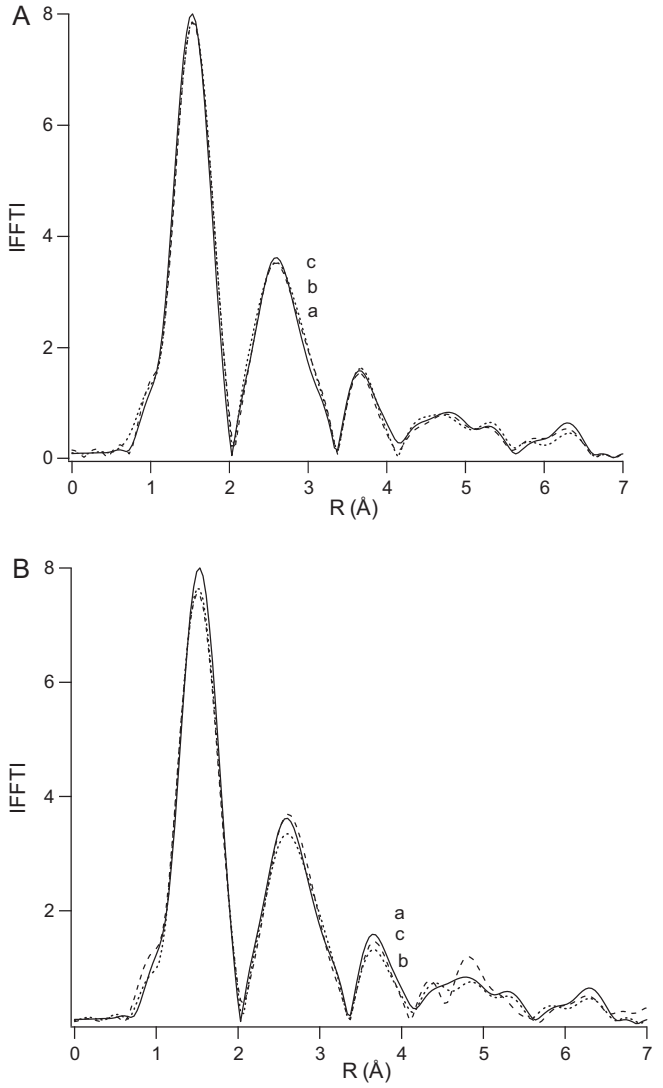

Fig. 5. (A) Co K-edge Fourier transforms EXAFS spectra (k^3-weighed, not phase corrected) of: (a) *CoPc* (___), (b) *CoPc/C* (...), (c) *FePc–CoPc/C* (- - -). (B) Co K-edge Fourier transforms EXAFS spectra (k^3-weighed, not phase corrected) of: (a) *CoPc* (___), (b) *CoPc/SiO_2* (...), (c) *FePc–CoPc/SiO_2* (- - -).

Upon heating *FePc/C(600)*, *CoPc/C(600)* and *FePc–CoPc/C(600)* to 800 °C to give *FePc/C(800)*, *CoPc/C(800)* and *FePc–CoPc/C(800)* metallic particles were generated on the carbon surface as shown by the appearance of the typical XRPD patterns of magnetite (i.e. cubic Fd−3m Fe_3O_4) [33], Co metal (i.e. cubic Fm−3m Co) [33] and a Fe–Co alloy (i.e. cubic Im−3m Fe–Co) [33–35], respectively (Fig. 9). An estimation of the particle mean size using the Scherrer equation has provided a significantly higher value (>10 nm) as compared to the EXAFS analysis, which may be due to a broad distribution of the metal particles [36].

Identical results were obtained by carrying out the thermo-diffraction study in situ under either nitrogen or argon in the temperature range from room temperature to 800 °C. Finally, it is worth mentioning that magnetite was the only crystalline iron containing compound also when the thermal treatment of *FePc/C* at 800° was carried out under a pure argon atmosphere, which confirms the important role played by the oxygenated species on the carbon surface.

To the best of our knowledge, XRPD studies of carbon supported metal phthalocyanines are limited to *CoPc* on Vulcan XC-72 [16]. For this species, the formation of (bcc) β-Co particles was detected for pyrolysis temperatures higher than 700 °C. As a further evidence of the importance of the support in governing the pyrolysis of Co–N_4 chelates, heat treatment of CoTETA/C (TETA = triethylentetraamine; C = porous carbon BP2000) at 800 °C has been reported to give an (fcc) α-Co phase [20].

3.2.4. Structural considerations

Incorporation of the TPD, XANES, EXAFS and XRPD data allows us to suggest a mechanism of pyrolysis of Ketjen Black-supported iron and cobalt phthalocyanines in the temperature range from 20 to 800 °C as well as assign a structure to the various metal-containing phases. Scheme 1 summarizes our interpretation of these data.

There is little doubt that the M-N_4 structure is preserved for both Fe and Co up to 600 °C, following the elimination of 1,2-benzodinitrile and phthalimide, but no discrimination between mixed- or single-metal units can be made at this stage. Indeed the formation of a statistical distribution of Fe–N_4 and Co–N_4 islands is equally likely. The analytical data unequivocally demonstrate that the extensive formation of metallic particles requires a temperature

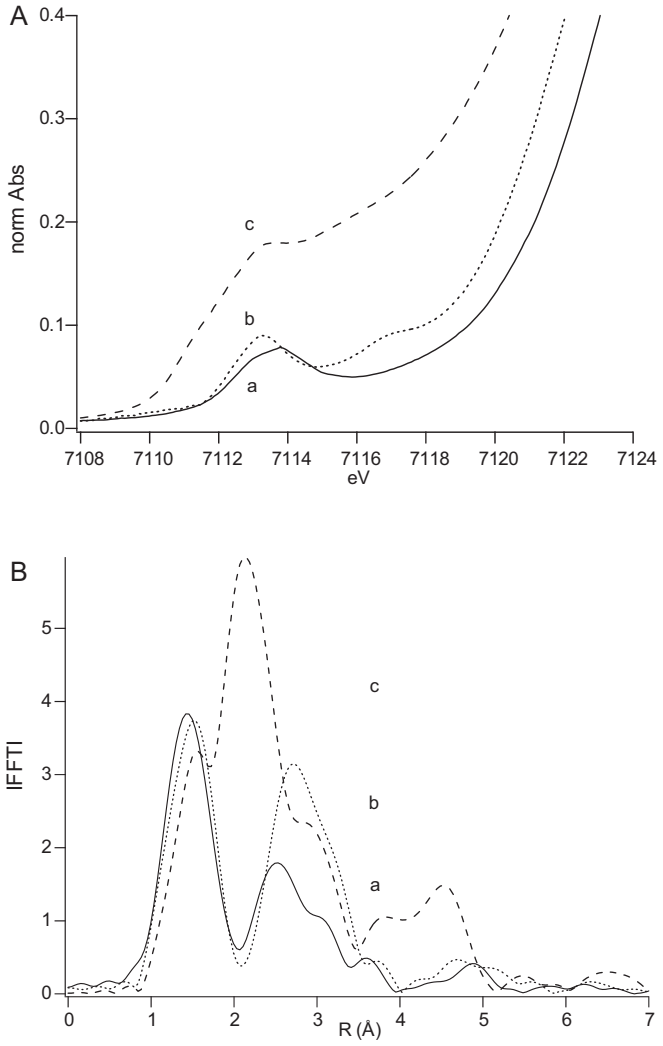

Fig. 6. (A) Fe K-edge normalised XANES spectra of: (a) *FePc–CoPc/C* (___), (b) *FePc–CoPc/C(600)* (...), (c) *FePc–CoPc/C(800)* (- - -). (B) Fe K-edge Fourier transforms EXAFS spectra (k^3-weighed, not phase corrected) of: (a) *FePc–CoPc/C* (___), (b) *FePc–CoPc/(600)* (...), (c) *FePc–CoPc/C(800)* (- - -).

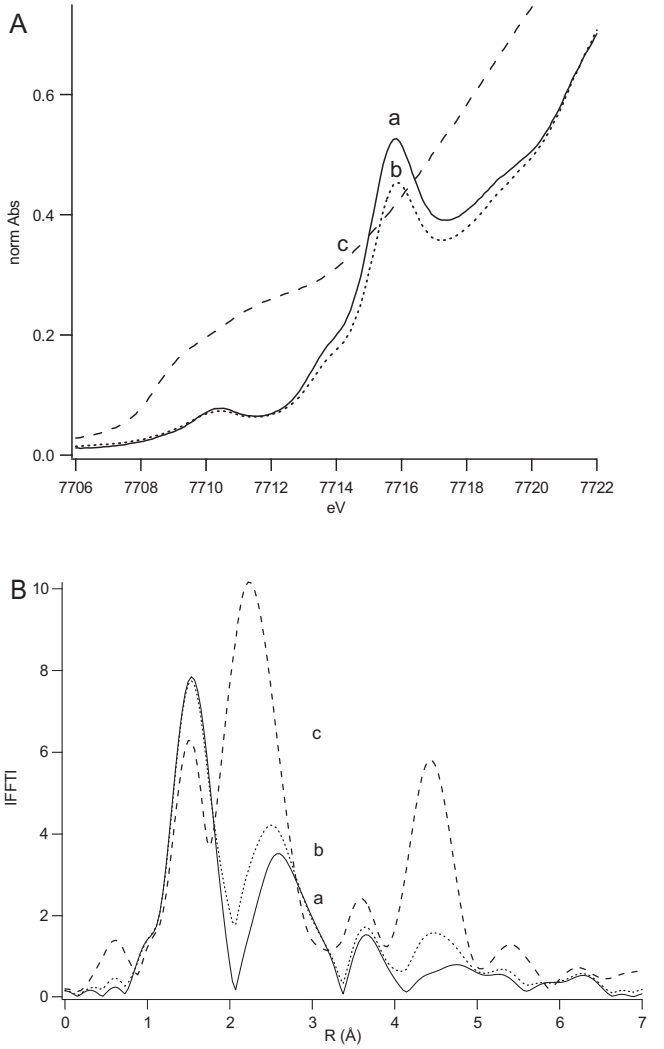

Fig. 7. (A) Co K-edge normalised XANES spectra of: (a) *FePc–CoPc/C* (___), (b) *CoPc/C(600)* (...), (c) *FePc–CoPc/C(800)* (- - -). (B) Co K-edge Fourier transforms EXAFS spectra (k^3-weighed, not phase corrected) of (a) *FePc–CoPc/C* (___), (b) *FePc–CoPc/(600)* (...), (c) *FePc–CoPc/C(800)* (- - -).

higher than 700 °C. Unlike *CoPc/C*, the pyrolysis of *FePc/C* at 800 °C leads to the formation of iron oxide, in the form of magnetite, even under ultra pure argon, which is a further evidence of the extensive presence of oxygenated groups on the carbon surface. Most interestingly, no trace of iron oxide is detected for *FePc–CoPc/C(800)* as only the peaks of a (*bcc*) Fe–Co alloy are displayed by the XRPD spectrum, though one cannot disregard the presence of a thin oxide coverage (see the EXAFS and XANES data) [34]. It is therefore likely that the surface of the (*bcc*) Fe–Co alloy is covered by cobalt with iron confined in the bulk.

The structural hypotheses presented in Scheme 1 are further corroborated by other studies previously reported; these include thermogravimetric analysis (TGA), time-of-flight secondary mass spectrometry (ToF-SIMS), X-ray photoelectron spectroscopy (XPS) and infrared spectroscopy (IR) [16–19]. In particular, a ToF-SIMS study of *FePc* and *CoPc* supported on Vulcan XC-72 has provided evidence of the maintenance of surface M-N_4 units up to 600 °C and the formation of metal, metal oxide and also metal carbide species at 800 °C [17,18]. Analogous conclusions were reached for *CoPc* supported on Vulcan XC-72 by XRD and IR spectroscopy [19].

3.3. Electrochemical studies

The electrochemical activity of *FePc/C(600)*, *CoPc/C(600)*, *FePc–CoPc/C(600)*, *FePc/C(800)*, *CoPc/C(800)* and *FePc–CoPc/C(800)* for the oxygen reduction reaction (ORR) was investigated by linear sweep voltammetry at room temperature (18–22 °C) using a rotating disc electrode (RDE). For all catalysts, the metal loading varied from 8 to 11 μg cm^{-2}, corresponding to 2.7–3.3 mg of ink. Two electrodes coated with different Pt catalysts were investigated for comparative purposes: a commercial *Pt/Vulcan* material by E-TEK (20 wt% Pt) with a metal loading of 32 μg cm^{-2} and a proprietary *Pt/C* material (3.2 wt% Pt) with a metal loading of 10 μg cm^{-2}. The former material has been purposefully selected because of its general use as cathode catalyst for the ORR for which it provides high mass activity and an exchange of less than $4e^-$ due to the contribution of the carbon support [42].

Before commenting the electrochemical data, it is worth recalling that the oxygen reduction may proceed through parallel two- and four-electron paths. As a general trend, *FePc* promotes the direct $4e^-$ ORR to water, while *CoPc* catalyzes the $2e^-$ path leading to H_2O_2 [4,5,43,44].

Relevant electrochemical parameters for the ORR catalyzed by the materials investigated in this work are reported in Table 5,

Table 5
Relevant electrochemical parameters for the ORR at room temperature on electrodes coated with the catalysts investigated in this work.[a]

Electrocatalyst	J_l, (mA cm^{-2})	V_{onset} (V vs. RHE)	S_a[d,e] (A gMet^{-1}) (0.95 V vs. RHE)	S_a[d,e] (A gMet^{-1}) (0.9 V vs. RHE)	V_{Tafel}[b] (mV dec^{-1})	Koutecky–Levich slope (mA cm^{-2} RPM$^{-1/2}$)	ne^{-}[c]
FePc/C(600)	−6.05	0.97	160	–	32	0.14234	4.0
CoPc/C(600)	−4.22	0.94	–	45	48	0.09803	2.8
FePc–CoPc/C(600)	−5.40	1.02	210	–	31	0.14185	4.0
FePc/C(800)	−4.68	1.02	102	–	34	0.12210	3.5
CoPc/C(800)	−3.89	0.98	–	145	53	0.08197	2.3
FePc–CoPc/C(800)	−4.41	1.01	76	346	46	0.11764	3.3
Pt/C	−4.76	1.00	–	65	94	0.12756	3.6
Pt/Vulcan	−4.61	1.15	63	113	72	0.12189	3.5

[a] Average values for at least three measurements.
[b] Corrected for diffusion–convection effects ($1/J = 1/J_l + 1/J_{kin}$).
[c] Values of Koutecky–Levich constants taken from [68] ($D = 1.95 \times 10^{-5}$ cm^2 s^{-1}; $\upsilon = 8.98 \times 10^{-3}$ cm^2 s^{-1}; $c_{ox} = 1.15 \times 10^{-3}$ M).
[d] Values of the mass-specific current columns not reported because out of the 10–80% range of I_L [43].
[e] An error of 5% was estimated in the measurements of the mass-specific current.

while the polarization curves are shown in Fig. 10. The experimentally determined limiting currents were within the ±10% limit theoretically established by the Levich equation [45].

From a perusal of the data reported in Table 5, one may readily realize that (i) irrespective of the metal composition and pyrolysis temperature, the ORR activity of the *Pc*-derived electrocatalysts is in the range of the best electrocatalysts reported so far; (ii) the activity of *FePc* and *FePc–CoPc/C*, heat treated at either 600 or 800 °C, is superior to that of the corresponding Co materials; (iii) the electrocatalysts obtained at 600 °C are fairly more active than those obtained at 800 °C. The complex nature of the present electrocatalysts did not allow us to determine the electroactive surface area, thus limiting the comparison with the Pt-based electrocatalysts. Therefore, we can only notice that the *Pc*-derived electrocatalysts exhibit higher ORR mass activity as compared to both *Pt/C* and *Pt/Vulcan*.

A superior performance of Fe and Co electrocatalysts, as compared to Pt, for the ORR has been previously observed in alkaline, acidic and neutral media [3–5,10–12,23,37–46]. Most of the reported data refer to molecular species, and only a few works deal with heat-treated macrocyclic compounds [13–19,22,47]. Likewise, the higher activity of *FePc* vs. *CoPc* has several precedents in the literature, irrespective of the structure of the electrocatalyst, i.e. phthalocyanine complexes [4–7,12,38,40,43,48,9,8], metal nanoparticles [22] or metal oxides [49–52]. It is worth noticing that the mixed-metal catalyst *FePc–CoPc/C(600)* is as active as *FePc/C(600)* which, however, contains about three times more iron (Table 1). This finding, in conjunction with the number of electron involved in the ORR process (*vide infra*), suggests the existence of a cooperative effect between the Fe and Co sites in *FePc–CoPc/C(600)*. Such a cooperation seems to hold also for the Fe–Co material pyrolyzed at 800 °C. While for the latter, the Fe–Co cooperation may be attributed to the formation of a Fe–Co alloy (in the absence of Co, a Fe_3O_4 phase is obtained in fact, see the XRPD spectra in Fig. 9), no sound explanation can be forwarded for the materials obtained at 600 °C where the carbon surface is likely covered by a random distribution of M-N_4 sites (Scheme 1). As pointed out by several authors, nitrogen functionalities in the carbon support (Vulcan) may have a role in the ORR activity in alkaline media [53–56].

Therefore, we cannot rule out that the functionalized Ketjen Black may contribute to the observed ORR activity, though no specific report has ever been reported.

The Tafel slopes for the ORR catalyzed by the materials investigated in this work are reported in Table 5. Three different sets of values have been observed in function of the metal: 31–35 mV dec^{-1}, 46–53 mV dec^{-1} and 74–94 mV dec^{-1} for Fe alone or combined with Co, Co and Pt, respectively. These data clearly indicate that the ORR mechanism depends on the metal, as also put in evidence by the different number of electrons involved in the ORR (Table 5). Indeed, Koutecky–Levich plots for all catalysts confirmed a prevailing 2e$^-$ reduction for Co and a 4e$^-$ reduction for Pt, Fe and its 1:1 alloy with Co, which is in good agreement with the literature [4,5,43–45].

The electrochemical stability of each catalyst was estimated by chronopotentiometry at a constant load of 2.5 mA cm^{-2}, corresponding to 250 A g^{-1} of metal. As shown in Fig. 11, with the exception of *Pt/C*, all catalysts showed a good stability with time.

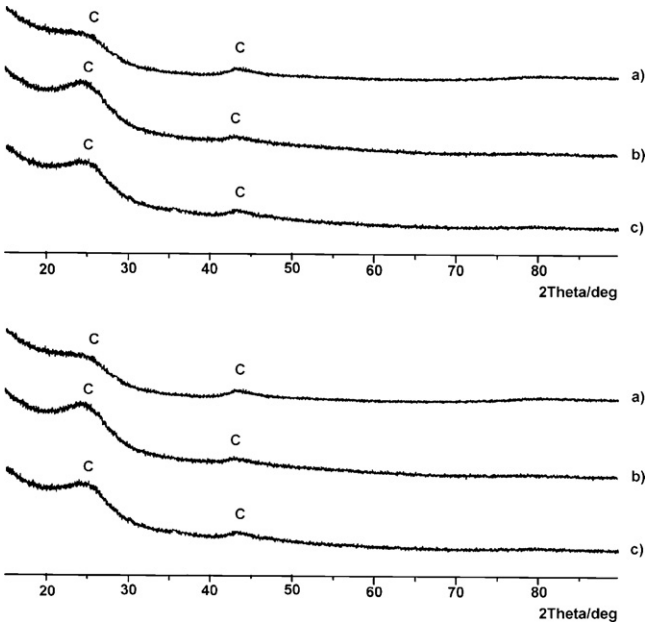

Fig. 8. XRD patterns of (a) Ketjen Black (C), (b) *FePc–CoPc/C* and (c) *FePc–CoPc/C(600)*.

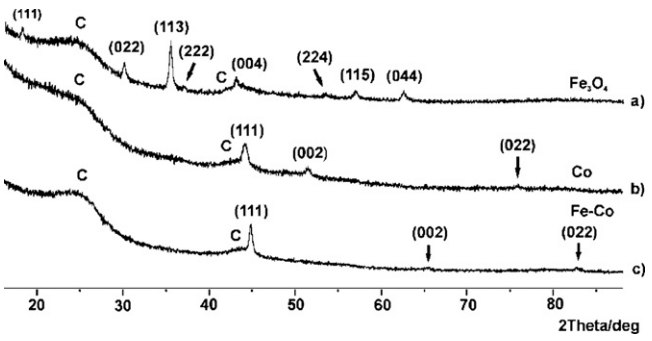

Fig. 9. XRD patterns of (a) *FePc/C(800)* (Fe_3O_4, cubic Fd−3m), (b) *CoPc/C(800)* (Co, cubic Fm−3m) and (c) *FePc–CoPc/C(800)* (Fe–Co alloy, cubic Im−3m).

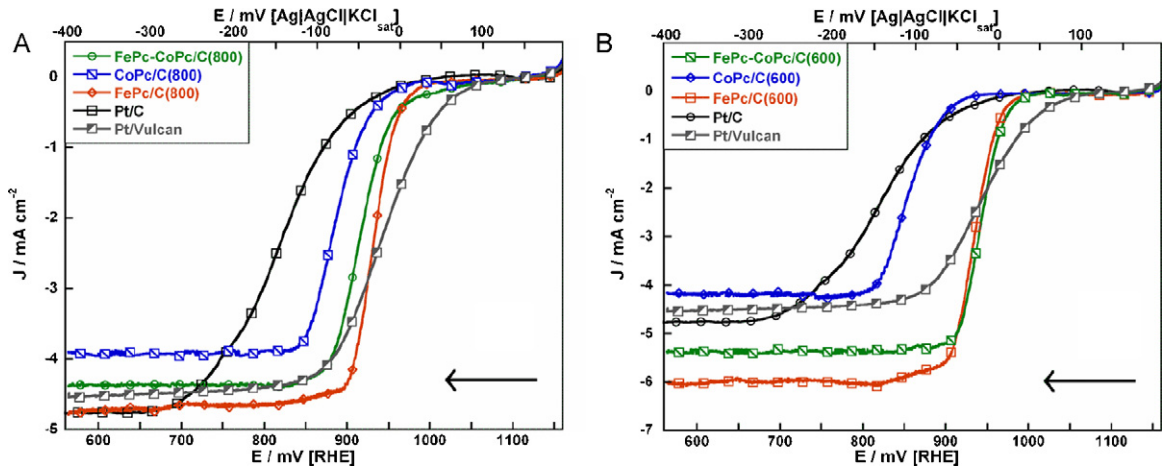

Fig. 10. Polarization curves for the ORR on the Fe and Co electrocatalysts obtained by pyrolysis at: (A) 800 °C, (B) 600 °C. Curves are also reported for *Pt/C* and *Pt/Vulcan*. Experimental conditions: KOH 0.1 M, O_2 saturated, RDE Ω = 1600 rpm, linear sweep voltammetry 5 mV s^{-1}, ref. electrode $AgCl|KCl_{sat}$ (all potentials are referred to RHE).

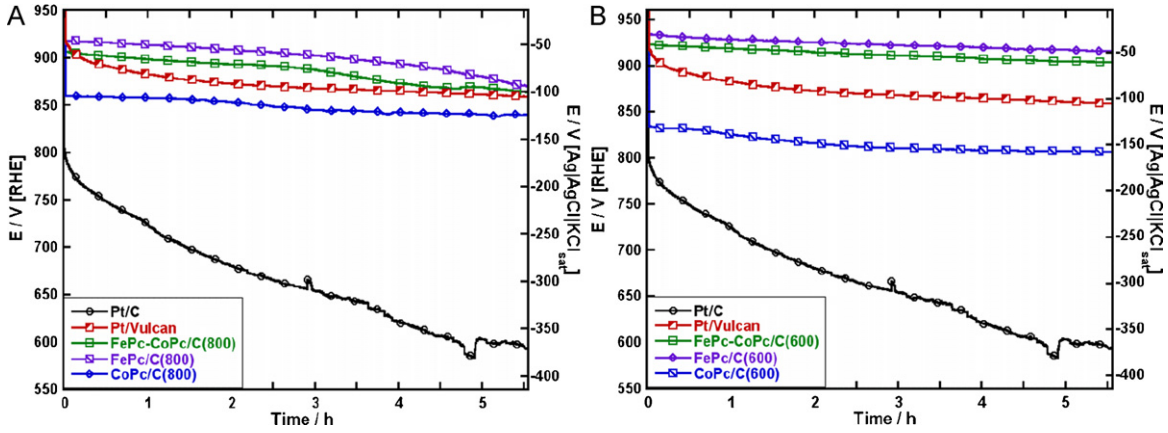

Fig. 11. Chronopotentiometric curves for the ORR catalyzed by the Fe and Co phthalocyanines heat treated at: (A) 800 °C, (B) 600 °C. Curves obtained with *Pt/C* and *Pt/Vulcan* are reported for comparative purposes. Experimental conditions: KOH 0.1 M, O_2 saturated, RDE Ω = 1600 rpm, constant current chronopotentiometry at 2.5 mA cm^{-2}, ref. electrode $AgCl|KCl_{sat}$ (all potentials are referred to RHE).

Experiments running for 16 h showed a voltage decay inferior to 10 mV h^{-1}. The catalyst obtained by heat treatment at 600 °C, in particular *FePc/C(600)* and *FePc–CoPc/C(600)*, gave the again the best performance, even better than that of the catalyst containing 20 wt% Pt.

A few ORRs have been performed in acidic media (1 M H_2SO_4) to explore the stability of the present *MPc*-based electrocatalysts in a different environment. A much lower stability than in alkaline media (just after three voltammetry cycles, the current density decayed by 70%) was observed for the materials obtained upon pyrolysis at 800 °C. A slightly better stability in acidic environment, not comparable to that in alkaline media however, was observed for the materials pyrolyzed at 600 °C for which different deactivation paths have been reported to occur [4,5,43,46].

Finally, the ORR activity of the heat-treated *MPc* materials was tested by adding increasing amounts of ethanol (from 1 to 10 wt%) into the oxygen saturated solution to mimic the potential effect of alcohol cross-over in direct alcohol fuel cells (DAFCs) [57–60]. None of the *Pc*-based electrocatalysts showed an appreciable sensitivity to the alcohol for concentrations as high as 5 wt%. Above this concentration, the current decreased, yet to a little extent (only 7% decay for an ethanol concentration of 10 wt%). Since none of the Fe and Co catalyst is able to oxidize ethanol in either half cells or monoplanar DAFCs [61–66], the current decay at high ethanol concentration may be ascribed to competitive adsorption of oxygen and ethanol on the catalytically active sites. In contrast, the ORR activity of *Pt/C* and *Pt/Vulcan* decreased dramatically just upon adding 1 wt% ethanol to the oxygen saturated solution [23,67], which is consistent with the well known ability of Pt-based catalysts to oxidize alcohols [68].

4. Conclusions

The impregnation of Ketjen Black (C) with iron and cobalt phthalocyanines (*MPc*) taken one by one or as a 1:1 stoichiometric mixture, followed by heat treatment at 600 °C under inert atmosphere, gave materials (*FePc/C(600)*, *CoPc/C(600)* and *FePc–CoPc/C(600)*) that contain single metal ions coordinated by four nitrogen atoms (M-N_4 units). Increasing the pyrolysis temperature to 800 °C resulted in the prevailing formation of carbon-supported, nanosized metal particles (*CoPc/C(800)* and *FePc–CoPc/C(800)*) or metal oxide (*FePc/C(800)*). A key role of the carbon support in determining the material structure at either temperature investigated was demonstrated by TPD, EXAFS, XANES and XRPD studies. These also showed that a Fe–Co alloy is obtained at 800 °C when the impregnation of Ketjen Black involves a mixture of *FePc* and *CoPc*.

Electrodes coated with the different Fe, Co and Fe–Co materials, containing very low metal loadings (from 8 to 11 μg cm^{-2}), were scrutinized for the oxygen reduction reaction (ORR) in alkaline media by linear sweep voltammetry. The electrochemical activity of all materials was further analyzed by Tafel and Koutecky–Levich

plots as well as chronopotentiometry. In view of the results obtained and a comparison with Pt-based electrocatalysts with different metal loadings, we feel to state that the Fe-containing electrocatalysts exhibit excellent activity for the ORR in alkaline media with convective limiting currents as high as 600 A g Fe^{-1} at room temperature and onset potentials as high as 1.02 V vs. RHE. In particular, we have found that (i) the ORR mass activity of the *Pc*-derived electrocatalysts is superior to that of the Pt catalysts investigated; (ii) the activity of *FePc* and *FePc–CoPc/C*, heat treated at either 600 or 800 °C, is superior to that of the corresponding Co materials; (iii) the electrocatalysts obtained at 600 °C are fairly more active than those obtained at 800 °C.

The excellent stability, the selective reduction of oxygen to water ($4e^-$ path) and the inability to oxidize alcohols makes the *FePc*-derived catalysts excellent candidates for manufacturing cathodes of DAFCs operating in alkaline media with anion-exchange membranes. Preliminary studies from this laboratory fully confirm the excellent performance of *FePc–CoPc/C(600)* in DAFCs fuelled with ethanol, glycerol and ethylene glycol [69].

Acknowledgments

It is acknowledged the financial support from the European Commission (Network of Excellence IDECAT, contract no. NMP3-CT-2005-011730), Regione Toscana (Progetto CESARE), CNR-Regione Lombardia "Mind in Italy" project and the MIUR (Italy) for the PRIN 2007 project 200775CREC-004. The ELETTRA synchrotron light laboratory in Basovizza (Trieste, Italy) and the staff of the XAFS beamline are gratefully acknowledged for the support and technical assistance.

References

[1] R. Jasinski, Nature 201 (1964) 1212.
[2] K. Oyazu, H. Murata, H. Yuesa, Macrocycles for Fuel Cell Cathodes, Springer-Verlag, Berlin, 2009, p. 139.
[3] B. Wang, J. Power Sources 152 (2005) 1.
[4] F. Van Den Brink, W. Visscher, E. Barendrecht, J. Electroanal. Chem. 157 (1983) 305.
[5] F. Van Den Brink, W. Visscher, E. Barendrecht, J. Electroanal. Chem. 175 (1984) 279.
[6] J.A.R. Van Veen, C. Visser, Electrochim. Acta 24 (1979) 921.
[7] E. Yeager, Electrochim. Acta 29 (1984) 1527.
[8] J. Zagal, M. Pàez, J. Electroanal. Chem. 339 (1992) 13.
[9] S. Baranton, C. Coutanceau, J.M. Lèger, C. Roux, P. Capron, Electrochim. Acta 51 (2005) 517.
[10] S. Baranton, C. Coutanceau, E. Garnier, J.M. Lèger, J. Electroanal. Chem. 590 (2006) 100.
[11] Z.P. Li, B.H. Liu, J. Appl. Electrochem. 40 (2010) 475.
[12] E. Hao Yu, S. Cheng, B.F. Logan, K.J. Scott, J. Appl. Electrochem. 39 (2009) 705.
[13] H. Kalvelage, A. Mecklenburg, U. Kunz, U. Hoffmann, Chem. Eng. Technol. 23 (2000) 803.
[14] M.C.M. Alves, J.P. Dodelet, D. Guay, M. Ladouceur, G. Tourillon, J. Phys. Chem. 96 (1992) 10898.
[15] S. Kim, G. Kwag, Bull. Korean Chem. Soc. 23 (2002) 25.
[16] M. Ladouceur, G. Lalande, D. Guay, J.P. Dodelet, J. Electrochem. Soc. 140 (1993) 1974.
[17] L.T. Weng, P. Bertrand, G. Lalande, D. Guay, J.P. Dodelet, Appl. Surf. Sci. 84 (1995) 9.
[18] G. Lalande, G. Faubert, R. Côté, D. Guay, J.P. Dodelet, L.T. Weng, P. Bertrand, J. Power Sources 61 (1996) 227.
[19] Y. Lu, R.G. Reddy, Int. J. Hydrogen Energy 33 (2008) 3930.
[20] H.J. Zhang, X. Yuan, W. Wen, D.Y. Zhang, L. Sun, Q.Z. Jiang, Z.F. Ma, Electrochem. Commun. 11 (2009) 206.
[21] H. Schulenburg, S. Stankov, V. Schunemann, J. Radnik, I. Dourbandt, S. Fiechter, P. Bogdanoff, H. Tributsch, J. Phys. Chem. B 107 (2003) 9034.
[22] X. Li, G. Liu, B.N. Popov, J. Power Sources 195 (2010) 6373.
[23] J.S. Spendelow, A. Wieckowski, Phys. Chem. Chem. Phys. 9 (2007) 2654.
[24] F. Coloma, A. Sepùlveda-Escribano, J.L.G. Fierro, F. Rodrìgues-Reinoso, Langmuir 10 (1994) 750.
[25] A. Guha, W. Lu, T.A. Zawodzinski Jr., D.A. Schiraldi, Carbon 45 (2007) 1506.
[26] S. Yang, G. Cui, S. Pang, Q. Cao, U. Kolb, X. Feng, J. Maier, K. Mullen, ChemSusChem 3 (2010) 236.
[27] I.T. Bae, D.A. Tryk, D.A. Scherson, J. Phys. Chem. B 102 (1998) 4114.
[28] B.N. Achar, K.S. Lokesh, G.M. Fohlen, T.M.M. Kumar, Reactive Funct. Polym. 63 (2005) 63.
[29] A. Bencini, D. Gatteschi, Transition. Met. Chem. 8 (1982) 1.
[30] J.K. Beattle, T.W. Hambley, J.A. Klepekto, A.F. Masters, P. Turner, Polyhedron 124 (2002) 2822.
[31] C.A. Melendres, J. Phys. Chem. 84 (1980) 1936.
[32] M. Carmo, A.R. Dos Santos, J.G.R. Poco, M. Linardi, J. Power Sources 173 (2007) 860.
[33] XRPD data were extracted from PDF-2 containing ICDD (International Centre for Diffraction Data) experimental powder data collection: http://www.icdd.com.
[34] Z.H. Wang, C.J. Choi, J.C. Kim, B.K. Kim, Z.D. Zhang, Mater. Lett. 57 (2003) 3560.
[35] Z.H. Wang, C.J. Choi, B.K. Kim, J.C. Kim, Z.D. Zhang, J. Alloy Compd. 351 (2003) 319.
[36] S. Calvin, S.X. Luo, C. Caragianis-Broadbridge, J.K. McGuinness, E. Anderson, A. Lehman, K.H. Wee, S.A. Morrison, L.K. Kurihara, App. Phys. Lett. 87 (2005) 233102.
[37] C. Coutanceau, M.J. Croissant, T. Napporn, C. Lamy, Electrochim. Acta 46 (2000) 579.
[38] J. Perez, E.R. Gonzales, E.A. Ticianelli, Electrochim. Acta 44 (1998) 1329.
[39] E. Hao Yu, S. Cheng, K. Scott, B. Logan, J. Power Sources 171 (2007) 275.
[40] L. Demarconnay, C. Cotanceau, J.M. Legèr, Electrochim. Acta 53 (2008) 3232.
[41] L. Genies, R. Faure, R. Durand, Electrochim. Acta 44 (1998) 1317.
[42] F.H.B. Lima, E.A. Ticianelli, Electrochim. Acta 49 (2004) 4091.
[43] F. Van Den Brink, W. Visscher, E. Barendrecht, J. Electroanal. Chem. 172 (1984) 301.
[44] I. Yamanaka, S. Tazawa, T. Murayama, R. Ichihashi, N. Hanaizumi, ChemSusChem 1 (2008) 988.
[45] K.J.J. Mayrhofer, D. Strmcnik, B.B. Blizanac, V. Stamenkovic, M. Arenz, N.M. Markovic, Electrochim. Acta 53 (2008) 3181.
[46] F. Van Den Brink, W. Visscher, E. Barendrecht, J. Electroanal. Chem. 157 (1983) 283.
[47] L. Zhang, J. Zhang, D.P. Wilkinson, H. Wang, J. Power Sources 156 (2006) 171.
[48] C.W.B. Bezerra, L. Zhang, H. Liu, K. Lee, A.L.B. Marques, E.P. Marques, H. Wang, J. Zhang, J. Power Sources 173 (2007) 891.
[49] A. Ishihara, Y. Ohgi, K. Matsuzawa, S. Mitsushima, K.I. Ota, Electrochim. Acta 55 (2010) 8005.
[50] E.R. Vago, E.J. Calvo, M. Stratmann, Electrochim. Acta 39 (1994) 1655.
[51] E.R. Vago, E.J. Calvo, J. Electroanal. Chem. 339 (1992) 41.
[52] E.R. Vago, E.J. Calvo, J. Electroanal. Chem. 338 (1995) 161.
[53] K. Gongo, F. Du, Z Xia, M. Durstock, L. Dai, Science 323 (2009) 760.
[54] Z. Chen, D. Higgins, Z. Chen, Carbon 48 (2010) 3057.
[55] T.C. Nagaiah, S. Kundu, M. Bron, M. Muhler, W. Schuhmann, Electrochem. Commun. 12 (2010) 338.
[56] Z. Chen, D. Higgins, Z. Chen, Electrochim. Acta 55 (2010) 4799.
[57] F.J.R. Varela, O. Savadogo, Asia-Pacific J. Chem. Eng. 54 (2009) 17.
[58] S. Baranton, C. Coutanceau, C. Roux, F. Hahn, J.M. Lèger, J. Electroanal. Chem. 577 (2005) 223.
[59] D. Chu, R. Jiang, Solid State Ionics 148 (2002) 591.
[60] K. Gadamsetti, S. Swavey, Dalton Trans. (2006) 5530.
[61] F. Viguer, S. Rousseau, C. Coutanceau, J.M. Léger, C. Lamy, Top. Catal. 40 (2006) 111.
[62] E. Antolini, J. Power Sources 170 (2007) 1.
[63] C. Bianchini, P.K. Shen, Chem. Rev. 109 (2009) 4183.
[64] V. Bambagioni, C. Bianchini, A. Marchionni, J. Filippi, F. Vizza, J. Teddy, P. Serp, M. Zhiani, J. Power Sources 190 (2009) 241.
[65] V. Bambagioni, C. Bianchini, J. Filippi, A. Marchionni, F. Vizza, P. Bert, A. Tampucci, Electrochem. Commun. 11 (2009) 1077.
[66] V. Bambagioni, M. Bevilacqua, C. Bianchini, J. Filippi, A. Marchionni, F. Vizza, L.Q. Wang, P.K. Shen, Fuel Cells 10 (2010) 582.
[67] L. Demarconnay, C. Cotanceau, J.M. Legèr, Electrochim. Acta 49 (2004) 4513.
[68] Y. Wang, D. Zhang, H. Liu, J. Power Sources 195 (2010) 3135.
[69] V. Bambagioni, M. Bevilacqua, J. Filippi, A. Marchionni, S. Moneti, F. Vizza, C. Bianchini, Chim. Oggi/Chem. Today 28 (VII) (2010).